Effect of alumina on microstructures of iron ore sinters from the perspective of the phase equilibria of the CaO-SiO_2-Fe_2O_3-Al_2O_3 system

Miyuki Hayashi[1], Amane Takahashi[2], Yukihiro Uchisawa[3], Takashi Watanabe[4] and Masahiro Susa[5]

1.Professor, Tokyo Institute of Technology, Tokyo 152-8552. E-mail: hayashi.m.ae@m.titech.ac.jp:
2.Student, Tokyo Institute of Technology, Tokyo 152-8552. E-mail: takahashi.a.az@gmail.com:
3.Student, Tokyo Institute of Technology, Tokyo 152-8552. E-mail: rintaro9773@gmail.com:
4.Assistant Professor, Tokyo Institute of Technology, Tokyo 152-8552. E-mail: watanabe.t.ai@m.titech.ac.jp:
5.Emeritus Professor, Tokyo Institute of Technology, Tokyo 152-8552. E-mail: susa.m.aa@m.titech.ac.jp:

Keywords: iron ore sinter, microstructure, silico-ferrite of calcium and aluminum, alumina, phase equilibria

ABSTRACT

Owing to the deterioration of iron ore, the Al_2O_3 concentration in iron ore increases, and thus it is important to investigate the effect of increment in Al_2O_3 concentration on the microstructures of iron ore sinters: During the sintering process, a melt is present in the sinter for only a few minutes, and thus, the microstructure of the sinter doesn't reach thermodynamic equilibrium. Nevertheless, the formation process of the microstructures can be interpreted and predicted to some extent from the equilibrium phase diagram. This study investigated the liquidus isotherm in the CaO-SiO_2-Fe_2O_3-5 mass%Al_2O_3 system at 1240°C in air and the phase equilibria of silico-ferrite of calcium and aluminum (denoted by SFCA) and SFCA-I by XRD and EPMA. The following results were obtained: (i) The ferrite melt region with a high Fe_2O_3 concentration shifts to the lower Fe_2O_3 side than the liquidus isotherm in the CaO-SiO_2-Fe_2O_3 system. (ii) The compositional region of SFCA extends in the $CaO{\cdot}3Fe_2O_3$-$4CaO{\cdot}3SiO_2$ direction than the silico-ferrite of calcium (denoted by SFC) composition region with a 0 mass%Al_2O_3. (iii) SFCA-I is observed in the present system, which suggests that the increment in the Al_2O_3 concentration contributes to the stability of SFCA-I. The results of (i)-(iii) imply that an increment in Al_2O_3 concentration in iron ore leads to a decrement in the volume fraction of the bonding phase and that the fraction of the SFCA phase increases, and those of $2CaO{\cdot}SiO_2$ and slag phases decrease in the bonging phase. The SFCA-I phase is also precipitated from the slag with an Al_2O_3 concentration around 5 mass%.

INTRODUCTION

The qualities of the sinter such as strength and reducibility affect the CO_2 emissions of the ironmaking process. Thus, the production of high-quality sinters is highly desirable. The quality depends significantly on the sinter microstructures (Oyama et al., 1996), which are composed of calcium ferrite, hematite, magnetite, and amorphous silicate (Sasaki and Hida, 1982; Scarlett et al., 2004; Patrick and Lovel, 2001). In particular, the silico-ferrite of calcium and aluminum (SFCA), consisting of CaO, SiO_2, Fe_2O_3, Al_2O_3, and MgO, plays the role of a bonding phase connecting the coarse hematite ores and contributes significantly to the quality of sinters (Hayes, Chen and Jak, 2016, I. Tonžetć and A. Dippenaar, 2011, Shigaki, I, Sawada, M, and Gennai, N, 1986).

During the sintering process, a melt is present in the sinter for only a few minutes which is a very short time for convection mass transfer, and consequently, the microstructure of the sinter cannot reach thermodynamic equilibrium. Nevertheless, the formation process of the microstructures, such as the melting and precipitation of SFCA, can be successfully interpreted and predicted from the equilibrium phase diagram of the CaO-SiO_2-Fe_2O_3 system, which is the main component of sinters (Hayashi, M, et al., 2022). Recently, the deterioration of iron ore has progressed, and the Al_2O_3 concentration in iron ores has increased. Thus, it is important to investigate the effect of Al_2O_3 on the compositional region of SFCA and the liquid phase as well as the phase equilibria, including SFCA in the CaO-SiO_2-Fe_2O_3-Al_2O_3 system to control the microstructures of sinters for the production of high-quality sinters.

To the best of our knowledge, however, there are no reports on the phase equilibria of the CaO-SiO_2-Fe_2O_3 system containing Al_2O_3 concentrations exceeding 1 mass% at temperatures below 1270 ˚C which can be attributed to the high viscosity of the high Al_2O_3-containing slag melt (Machida, et al., 2005) which results in slow mass transfer and reaction rates, and thus a long time is required for the system to reach equilibrium. SFCA may precipitate at temperatures lower than 1300 ˚C during the cooling cycle of the sintering process. (Sasaki and Hida, 1982) Thus, a phase diagram with such a high Al_2O_3 concentration at temperatures lower than 1270 ˚C may be necessary to control the microstructure of the sinter and produce high-quality sinters.

This study investigates the effect of Al_2O_3 on the compositional regions of SFCA and the liquid phase, and the phase equilibria including SFCA in a CaO-SiO_2-Fe_2O_3-5mass%Al_2O_3 system at 1240 ˚C in air (Takahashi, A, et al., 2023) and estimates the effect of alumina on microstructures of iron ore sinters.

EXPERIMENTAL

TABLE 1 lists the chemical composition of the samples. The samples were prepared from reagent-grade $CaCO_3$, SiO_2, Fe_2O_3, and Al_2O_3 powders. To obtain the desired compositions, the reagents were weighed and then mixed using an alumina mortar and pestle.

TABLE 1 – Initial compositions of the samples.

Sample No.	Composition (mass%)				Ratio (at%)	
	CaO	SiO_2	Fe_2O_3	Al_2O_3	Ca/Si	Fe/Si
1	29.45	15.20	50.35	5.00	2.08	0.62
2	24.00	9.00	62.00	5.00	2.86	1.30
3	24.00	7.50	63.50	5.00	3.43	1.59
4	19.92	9.36	65.72	5.00	2.28	1.32
5	24.00	4.80	66.20	5.00	5.36	2.59
6	18.81	5.17	71.06	5.00	3.90	2.59
7	18.81	3.00	73.19	5.00	6.72	4.59
8	12.90	7.60	74.50	5.00	1.82	1.84
9	18.81	1.50	74.69	5.00	13.44	9.37
10	16.50	0.00	77.00	5.00	-	-
11	11.83	1.34	81.84	5.00	9.46	11.49
12	6.96	1.56	86.49	5.00	4.78	10.43
13	5.39	0.00	89.61	5.00	-	-
14	18.53	16.58	62.40	2.50	1.20	0.71

The sample holder was prepared by spirally winding a Rh/Pt wire (0.5 mm diameter, 13 mass%) (Hayes, Chen and Jak, 2016), on which a sample mixture (approximately 0.4 g), which was uniaxially cold-pressed to a tablet diameter of 10 mm, was placed. Using a spiral sample holder, the molten sample was maintained in the form of a film between the gaps of the wire by surface tension during the equilibrium experiment, to ensure good contact with water during quenching and prevent crystallization (Hayes, Chen and Jak, 2016). A sample tablet placed on the sample holder was suspended using the same wire in the maximum temperature zone of the furnace and was maintained at 1240 °C for more than 48 h in air to attain equilibrium: preliminary experiments indicate that 48 h is sufficient for the samples to reach equilibrium at 1240ºC. As for samples No. 1, 3, 4, and 8, a sample was kept at 1300 ˚C or higher for more than 30 min to promote mass transfer. After that,

the furnace temperature was lowered to 1240 °C (the equilibrium temperature) at a rate of 1 °C/min, and then the sample was kept at that temperature for more than 48 h in air to attain equilibrium. After equilibration, the crucible containing the sample was quenched into water. For samples No. 11-13 (which have no equilibrium liquid phase), the sample mixture was uniaxially pressed to form a tablet. The tablet was placed in a Pt crucible and heated at 1240 °C in air for at least 24 h. Then, the tablet was thoroughly crushed and mixed. The mixture was uniaxially pressed to form a tablet and heated in the same manner. The heat treatment was repeated three times. Metastable phases such as calcium aluminate and gehlenite were formed in the sample after one heat treatment; however, these phases disappeared after two or three treatments, thus indicating that the sample reached equilibrium.

Each obtained sample was divided into two parts: one was pulverized into a powder and analyzed by XRD to determine the phase present, and the other part was analyzed by an EPMA to observe the microstructure and for compositional analysis. The XRD analyses were carried out with CuKα radiation at an accelerating voltage of 40 kV and a filament current of 250 mA. The diffraction scanning rate was 0.005°/step or 0.02°/step, at 1°/min or 5°/min, and the diffraction angle 2θ was between 5° and 70°. The microstructures were measured by EPMA at an accelerating voltage of 15 kV and a probe current of 3 nA for the backscattered electron images (BEI), and 20 or 50 nA for elemental mapping, where the analysis area was ϕ1 μm. The composition of each phase was quantitatively analyzed by point analysis, where the analysis area was ϕ5 μm for some liquid phases and ϕ1 μm for others. The ZAF2 correction was performed. For quantitative analyses by EPMA, a glassy sample of 32.83CaO-35.71SiO_2-24.46Fe_2O_3-5.00Al_2O_3-2.00MgO (mass%) was used as the standard sample.

RESULTS

Table 2 shows the measured compositions of the phases. FIG 1 shows a plot of the measured composition of the phases of each sample projected onto the CaO-SiO_2-Fe_2O_3-5mass%Al_2O_3 plane. SFCA contained Al_2O_3 concentrations in the range of 5.47–9.35mass% and the Al_2O_3 concentrations in the liquid and SFCA-I in equilibrium with SFCA were lower than those of SFCA, thus indicating that the preferential distribution of Al_2O_3 in SFCA. However, when SFCA-I is in equilibrium with the liquid or hematite, and SFCA is not present, the Al_2O_3 concentration in SFCA-I can reach 9.59 mass%, which is much higher than that of SFCA-I equilibrated with SFCA. The SiO_2 concentration of SFCA-I is lower than that of SFCA. In this study, the SiO_2 concentrations of SFCA-I and SFCA were 0.00–1.31mass% and 1.55–6.30mass%, respectively. In FIG 1, samples No. 1-3, 5-7 and 9 indicate equilibria between Liquid and SFCA. The liquid phase compositions have a C/S ratio of larger than 2, which is a critical ratio determining the saddle point between the two liquid regions on the Alkemade join between Fe_2O_3 and $2CaO{\cdot}SiO_2$ (denoted by C_2S). The presence of the saddle point is predicted by thermodynamic theory. Nevertheless, it is noteworthy that the liquid phase compositions of samples No. 4 and 8 have a C/S ratio of less than 2, which suggests that the SFCA primary phase field exists in the low C/S region. FIGs 2 and 3 show the XRD profiles and elemental mappings of samples No. 4 and 8, respectively. As shown in FIGs 2 and 3, the solid precipitations during the cooling cycles are not observed in liquid phases. The phenomenon that the SFCA primary phase field extends to the low C/S region may be relevant to the high Al_2O_3 concentration: a part of Fe ions in the SFCA phase with high Al_2O_3 concentrations may be Fe^{2+} ions by the reaction $2(Fe^{3+}, Al^{3+}) = (Ca^{2+}, Fe^{2+}) + Si^{4+}$ (Patrick and Pownceby, 2002). Thus, the stable compositional region of SFCA extends to the lower C/S.

SFCA-I was formed in samples No. 7, 9-11, and 13. In this study, the presence of SFCA-I was confirmed by XRD and EPMA. For example, FIG 4(a) shows the XRD profile of sample No. 11. In addition to the SFCA-I peaks, hematite and SFCA peaks were observed in this sample. FIG 4(b) and 4(c) show the XRD profiles of sample No. 7. FIG 5(a) and (b) show the elemental mappings of samples No. 11 and 7, respectively, where SFCA-I and SFCA coexist. The brightest phase with the highest Fe concentration in the BEI of No. 11 was hematite. In samples No. 11 and 7, SFCA and SFCA-I exhibited almost the same brightness, and the BEIs were not sufficient to distinguish them. Thus, they were distinguished based on the differences in the concentration of each element. SFCA-I is in the Fe- and Ca-rich and Al- and Si-poor regions, while SFCA is in the Fe- and Ca-poor regions and the Al- and Si-rich regions.

TABLE 2 – Measured compositions of the phases.

Sample No.	Phases	Composition (mass%)				Ratio (mass%)
		CaO	SiO_2	Fe_2O_3	Al_2O_3	CaO/SiO_2
1	Liquid	35.45	22.18	38.29	4.08	1.60
	SFCA	16.38	6.30	70.77	6.55	2.6
	C_2S	64.04	35.18	0.78	0.00	1.82
2	Liquid	30.76	8.29	57.94	3.00	3.71
	SFCA	15.45	4.54	74.21	5.80	3.40
	C_2S	64.97	33.05	1.98	0.00	1.97
3	Liquid	29.70	8.81	58.00	3.49	3.37
	SFCA	15.41	4.31	72.49	7.79	3.58
4	Liquid	35.76	26.26	34.07	3.90	1.36
	SFCA	15.19	5.94	72.92	5.94	2.56
5	Liquid	28.17	4.85	63.29	3.69	5.81
	SFCA	15.11	3.53	73.85	7.51	4.28
6	Liquid	29.75	6.88	60.62	2.75	4.32
	SFCA	15.24	4.32	74.96	5.47	3.53
7	Liquid	26.82	3.40	66.91	2.87	7.89
	SFCA	13.89	3.07	76.77	6.27	4.52
	SFCA-I	16.08	1.31	79.74	2.87	12.3
8	Liquid	35.83	29.56	28.63	5.99	1.21
	SFCA	14.85	6.13	71.31	7.71	2.42
	Hematite	0.21	0.02	98.42	1.36	10.5
9	Liquid	23.89	1.38	71.97	2.77	17.31
	SFCA	13.16	2.09	78.18	6.58	6.30
	SFCA-I	13.82	0.53	80.57	5.08	26.08
10	Liquid	23.81	0.00	73.47	2.72	-
	SFCA-I	13.94	0.00	80.89	5.16	-
11	SFCA	12.50	1.55	80.24	5.71	8.06
	SFCA-I	12.86	0.38	82.09	4.67	33.84
	Hematite	0.35	0.01	98.65	0.99	35
12	SFCA	13.54	2.79	74.32	9.35	4.85
	Hematite	0.15	0.04	98.32	1.49	3.75
13	SFCA-I	11.96	0.00	78.45	9.59	-
	Hematite	0.13	0.00	97.87	2.00	-
14	Liquid	34.50	31.16	29.98	4.36	1.11
	Hematite	0.13	0.02	98.96	0.89	6.5
	CS	47.20	52.00	0.81	0.00	0.91

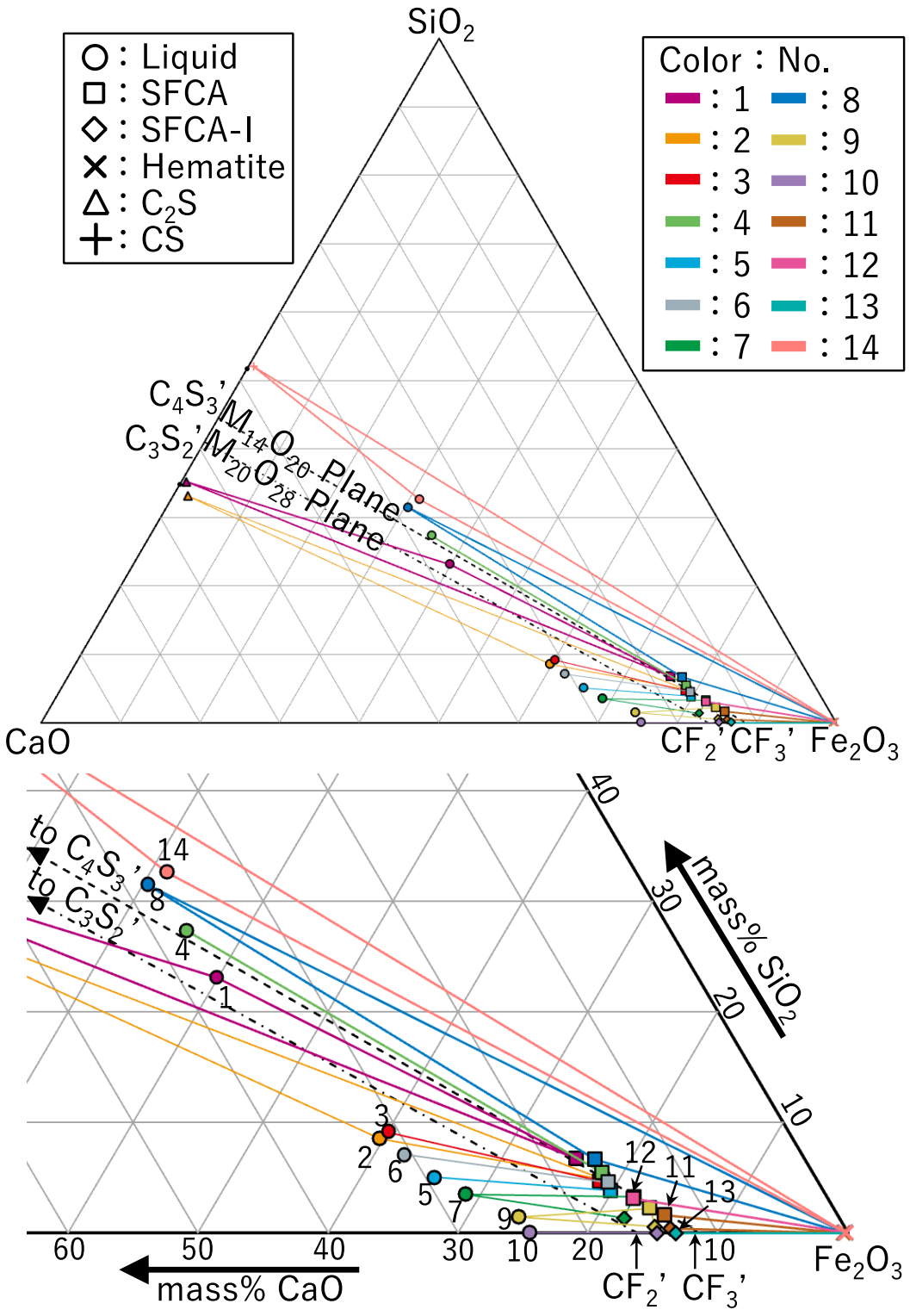

FIG 1 – Measured compositions of the phases for samples No. 1-14 on the iron-rich corner of the CaO-SiO_2-Fe_2O_3-5 mass%Al_2O_3 system in air at 1240°C (Takahashi et al., 2023).

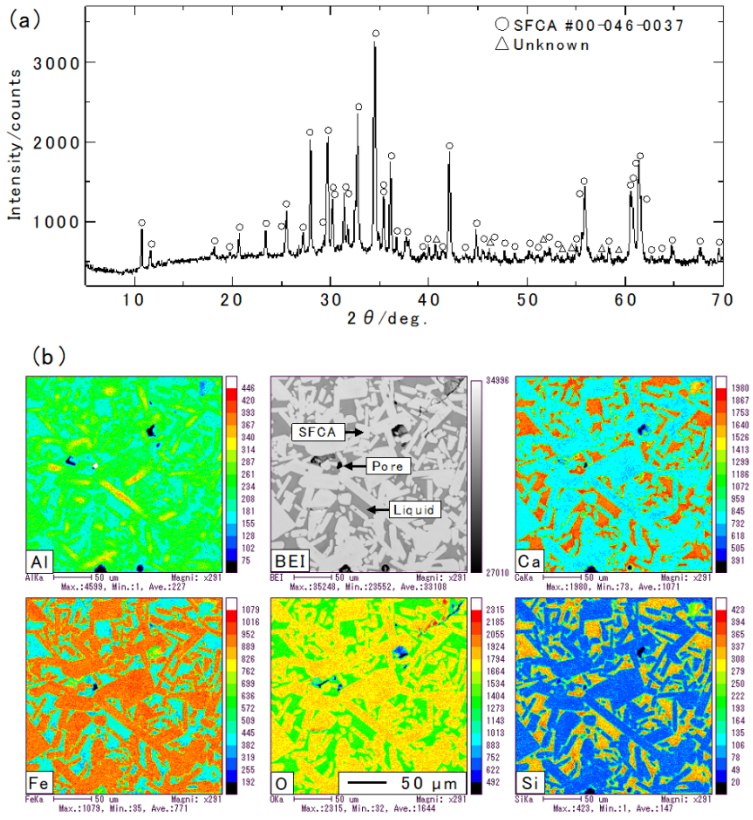

FIG 2 – XRD profile and elemental mappings of sample No. 4.

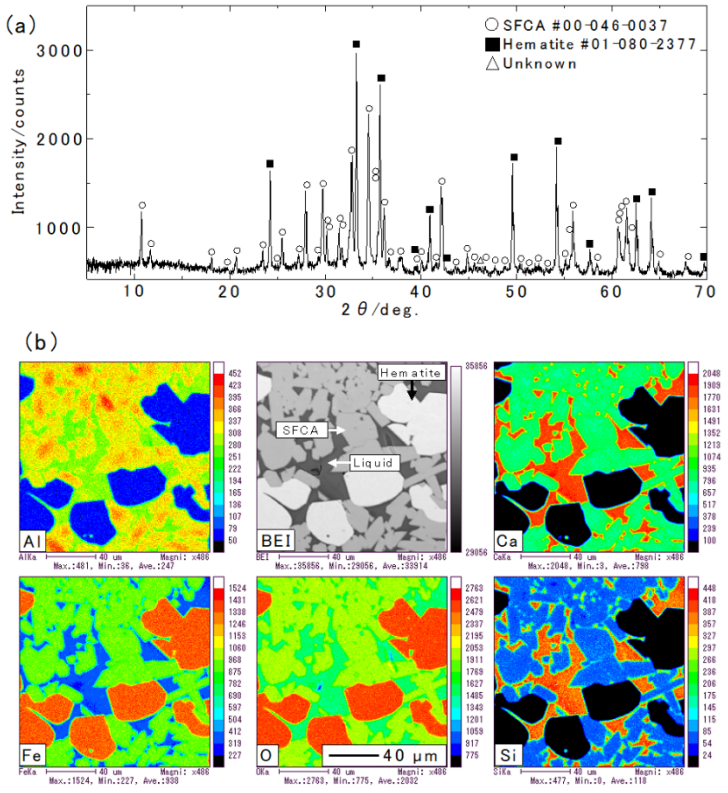

FIG 3 – XRD profile and elemental mappings of sample No. 8.

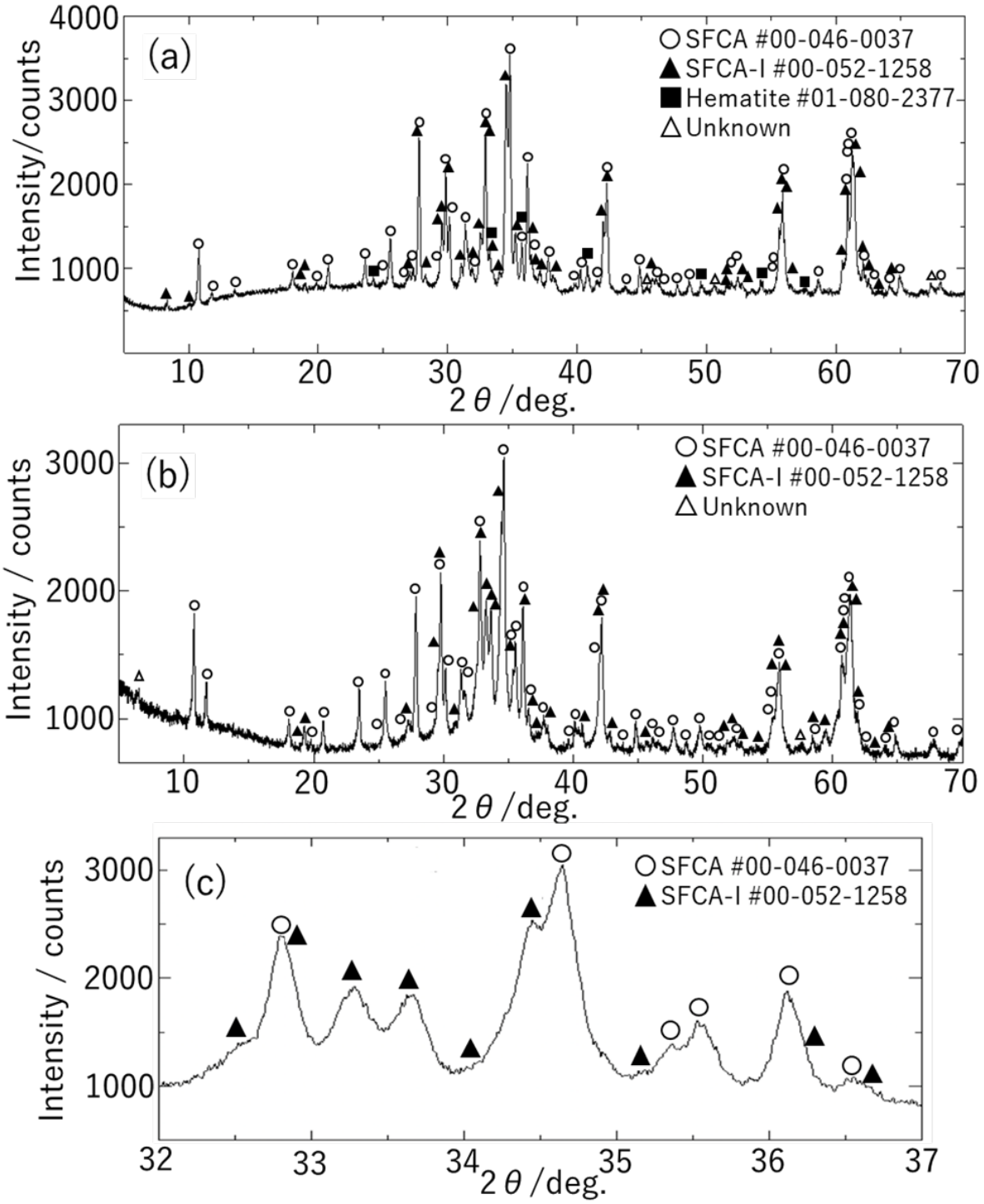

FIG 4 – (a) XRD pattern of sample No. 11, (b) XRD pattern of sample No. 7, and (c) XRD pattern of sample No. 7 ($2\theta = 32^{o} - 37^{o}$) (Takahashi et al., 2023).

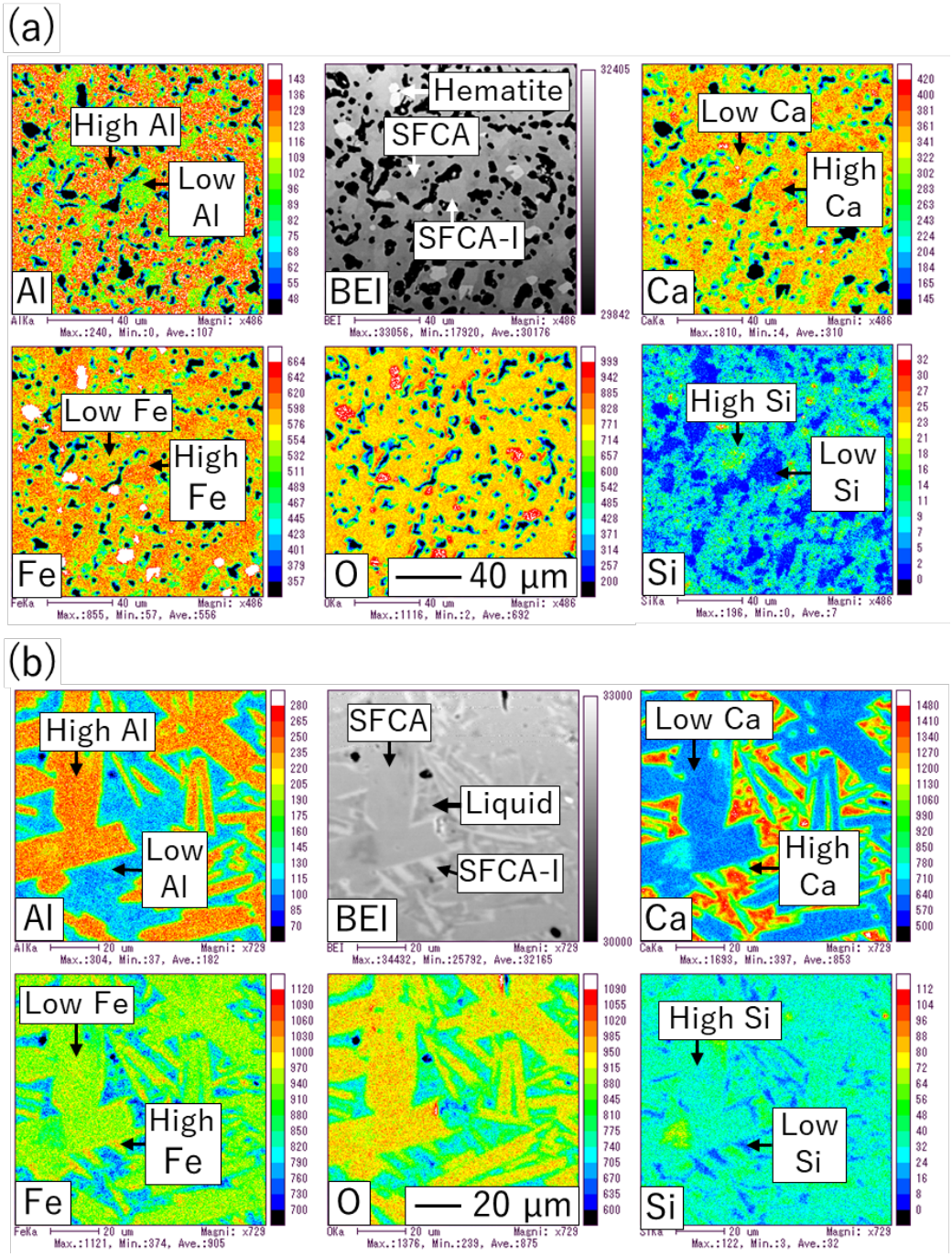

FIG 5 – (a) Mapping analysis of sample No. 11, (b) Mapping analysis of sample No. 7 (Takahashi et al., 2023).

DISCUSSION

In this study, the initial composition was CaO-SiO_2-Fe_2O_3-5mass%Al_2O_3. However, since Al_2O_3 was preferentially distributed in SFCA, an Al_2O_3 concentration higher than 5 mass% was obtained. FIG 6 shows the relationship between the mass ratio of CaO/SiO_2 (denoted by C/S) and the Al_2O_3 concentration for the SFCA compositions. Chen et al. (2019) reported that the C/S ratio of the SFC composition region is in the range of 2.92 to 4.322, which are plotted in FIG 6 as values at 0 mass% Al_2O_3. The highest C/S ratio of the SFCA composition region at 5 mass% Al_2O_3 was determined by interpolation using a straight line drawn by connecting the results of Chen et al. (2019) and those of this study, while the lowest C/S ratio was determined using a straight line drawn by the least-square fitting of four plots obtained in this study, passing through the plot of Chen et al. (2019) at 0 mass%

Al_2O_3. It was thus found that the C/S ratio of the SFCA compositional region was in the range of 2.77 to 7.60 at 5 mass% Al_2O_3. FIG 6 reveals the expansion of the SFCA compositional region upon the addition of Al_2O_3 which is also consistent with the results of Patrick and Pownceby (2002), while the compositional region of the SFCA with 5 mass% Al_2O_3 determined in this study was even wider than that reported by Patrick and Pownceby.

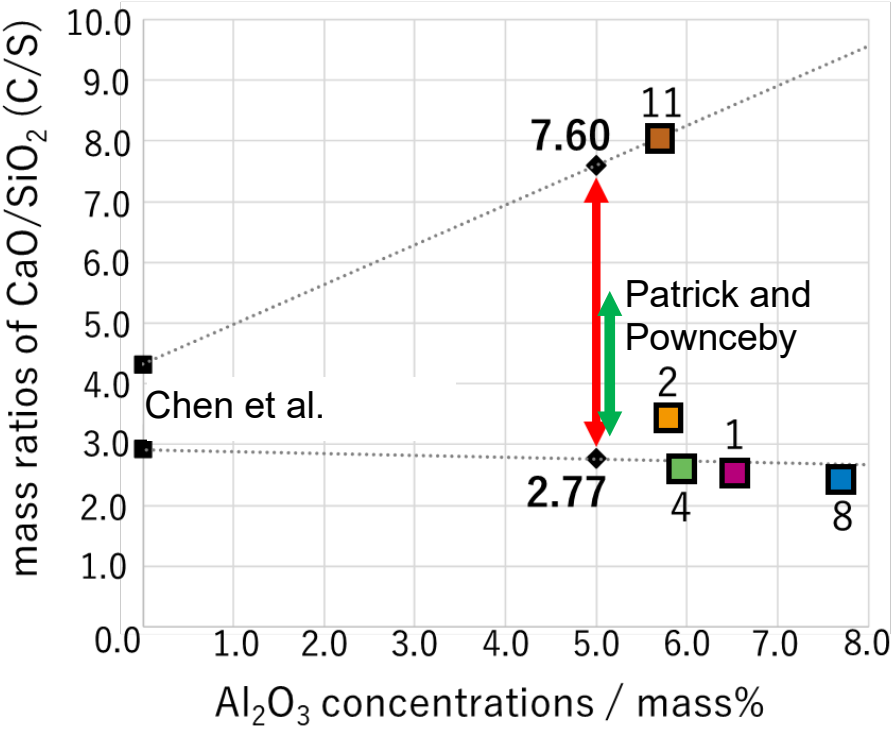

FIG 6 – Estimation of the SFCA composition range in 5 mass%Al_2O_3.

FIG 7 shows the isothermal cross-section of the CaO-SiO_2-Fe_2O_3-5mass%Al_2O_3 at 1240°C superimposed on that of the CaO-SiO_2-Fe_2O_3 system reported by Chen *et al*. (2019) and the liquidus isotherm in the CaO-SiO_2-Fe_2O_3 system reported by Slag Atlas (1995). Compared to these systems, the liquidus isotherm in the CaO-SiO_2-Fe_2O_3-5mass%Al_2O_3 system shifted toward a low Fe_2O_3. This shift attributed to the addition of Al_2O_3 is consistent with the results of Cheng *et al*. (2021), who investigated the CaO-Fe_2O_3-Al_2O_3 system, and those of Chen *et al*. (2021), who studied the effects of the addition of 1, 2, and 4 mass% Al_2O_3 on the CaO-SiO_2-Fe_2O_3 system. Furthermore, Yang *et al*. (1978) reported that the addition of 2 mass%Al_2O_3 shifted the composition range of the silicate melt toward low Fe_2O_3 in the CaO-SiO_2-Fe_2O_3-2mass%Al_2O_3 system at 1300°C. Thus, the results of the present study are consistent with those of the previous studies, thus indicating that the addition of Al_2O_3 contributes to the shift of the liquid-phase line to the low Fe_2O_3 side.

The endpoints of the low Fe_2O_3 side of the SFCA composition region were in equilibrium with the liquid phase, C_2S, and hematite, whereas those of the high Fe_2O_3 side were in equilibrium with hematite and SFCA-I. The SFCA-I compositional region existed in a region with a lower SiO_2 concentration than that of the SFCA compositional region. The endpoint of the low Fe_2O_3 side of the SFCA-I compositional region was in equilibrium with SFCA and the liquid phase. The high Fe_2O_3 endpoint with the low-CaO side was in equilibrium with hematite, and that with the high-CaO side was in equilibrium with the liquid phase. Chen *et al*. (2021) reported that the endpoints on the high Fe_2O_3 side of SFCA at 1255°C and 1265°C for 1 mass% Al_2O_3 and at 1275°C for 2 mass%Al_2O_3 were in equilibrium with the liquid phase and hematite, suggesting that SFCA-I did not exist. The results of this study suggest that the addition of Al_2O_3 contributes to the stability of SFCA-I in the CaO-SiO_2-Fe_2O_3 system.

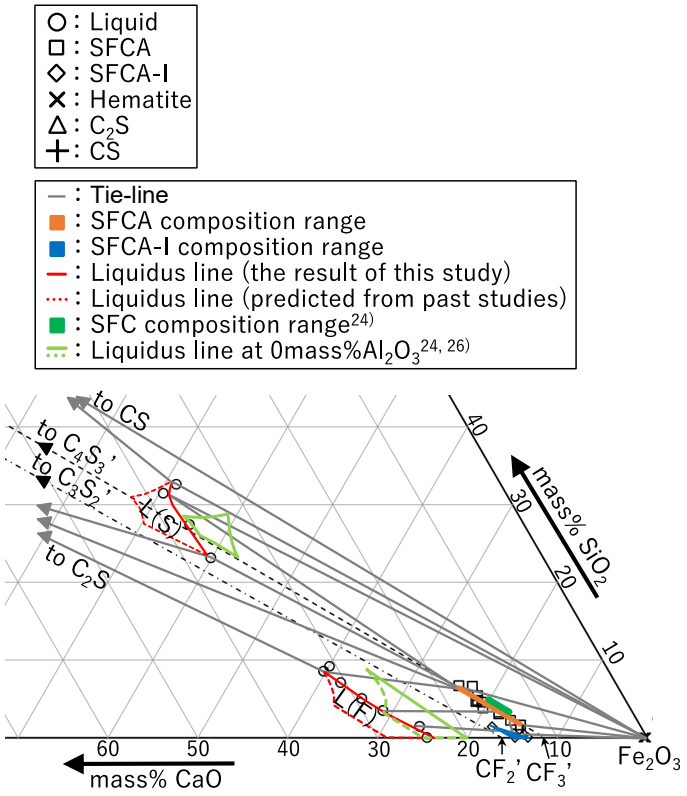

FIG 7 – Isothermal section of the $CaO\text{-}SiO_2\text{-}Fe_2O_3\text{-}5mass\%Al_2O_3$ system in air at 1240 °C based on the present study and its comparison with previous studies. (Chen et al., 2019, Dayal and Glasser, 1967) (Takahashi, et al. 2023).

Let us consider the microstructure formation of iron ore sinters from the perspective of the phase diagram of the $CaO\text{-}SiO_2\text{-}Fe_2O_3$ system reported by Chen et al. (2019). FIG 8(a) shows the phase equilibrium of the iron-rich corner of the $CaO\text{-}SiO_2\text{-}Fe_2O_3$ system in air including liquidus, the SFC and C_2S primary phase fields, the SFC solid solution, and a common iron ore composition (Chen et al., 2019). The straight lines connecting $4CaO{\cdot}3SiO_2$ (denoted by C_4S_3, not present as a compound) and $CaO{\cdot}3Fe_2O_3$ (denoted by CF_3, not present as a compound), and SiO_2 and iron ore composition are denoted by Line A and Line B, respectively. SFC solid solution is on Line A. T1 and T2 correspond to the temperatures at the intersections of the boundary between SFC (SFCA) and Fe_2O_3 primary phase fields with the extensions of straight lines connecting LC(1) and Fe_2O_3, and LC(2) and Fe_2O_3, respectively. T3 corresponds to the eutectic temperature of SFC (SFCA), Fe_2O_3 and C_2S. In general, some SiO_2 gangue minerals in iron ore remain unreacted during sintering, and the local composition of iron ore sinter shifts away from the SiO_2 corner of the $CaO\text{-}SiO_2\text{-}Fe_2O_3$ system along Line B. FIG 8(b) shows schematic illustrations of the equilibrium microstructures for LC (1) and LC (2). For both compositions, Fe_2O_3 and liquid phases are equilibrated at 1300°C, and then during the cooling cycle, SFC (SFCA) phases are precipitated from the liquid phase at T1 and T2 for LC (1) and LC (2), respectively. For LC (1), when the temperature decreases to T3, C_2S is precipitated from the residual liquid. On the other hand, as for LC (2), Fe_2O_3 and SFC (SFCA) phases are equilibrated below T2. Because Lines A and B approach each other as the C/S ratio is larger, the fraction of SFC (SFCA) is larger for LC (2) than for LC (1).

The effect of alumina on microstructures of iron ore sinters can be estimated from FIG 7: The liquidus isotherm in the $CaO\text{-}SiO_2\text{-}Fe_2O_3\text{-}5mass\%Al_2O_3$ system shifted toward a low Fe_2O_3 than that in the $CaO\text{-}SiO_2\text{-}Fe_2O_3$ system. Thus, an increment in Al_2O_3 concentration in iron ore leads to a decrement in the volume fraction of the bonding phase. It can also be found from FIG 7 that the compositional region of SFCA extends in the $CaO{\cdot}3Fe_2O_3\text{-}4CaO{\cdot}3SiO_2$ direction than the silico-ferrite of calcium (denoted by SFC) composition region with a 0 $mass\%Al_2O_3$. The compositions of the iron ore sinters are heterogeneous from place to place, with local compositions extending from the LC(1) to LC(2) composition range or beyond. Thus, the expansion of the compositional range of SFCA from SFC

implies that the fraction of the SFCA phase increases, and those of $2CaO \cdot SiO_2$ and slag phases decrease in the bonding phase. The SFCA-I phase is also precipitated from the slag with an Al_2O_3 concentration around 5 mass%.

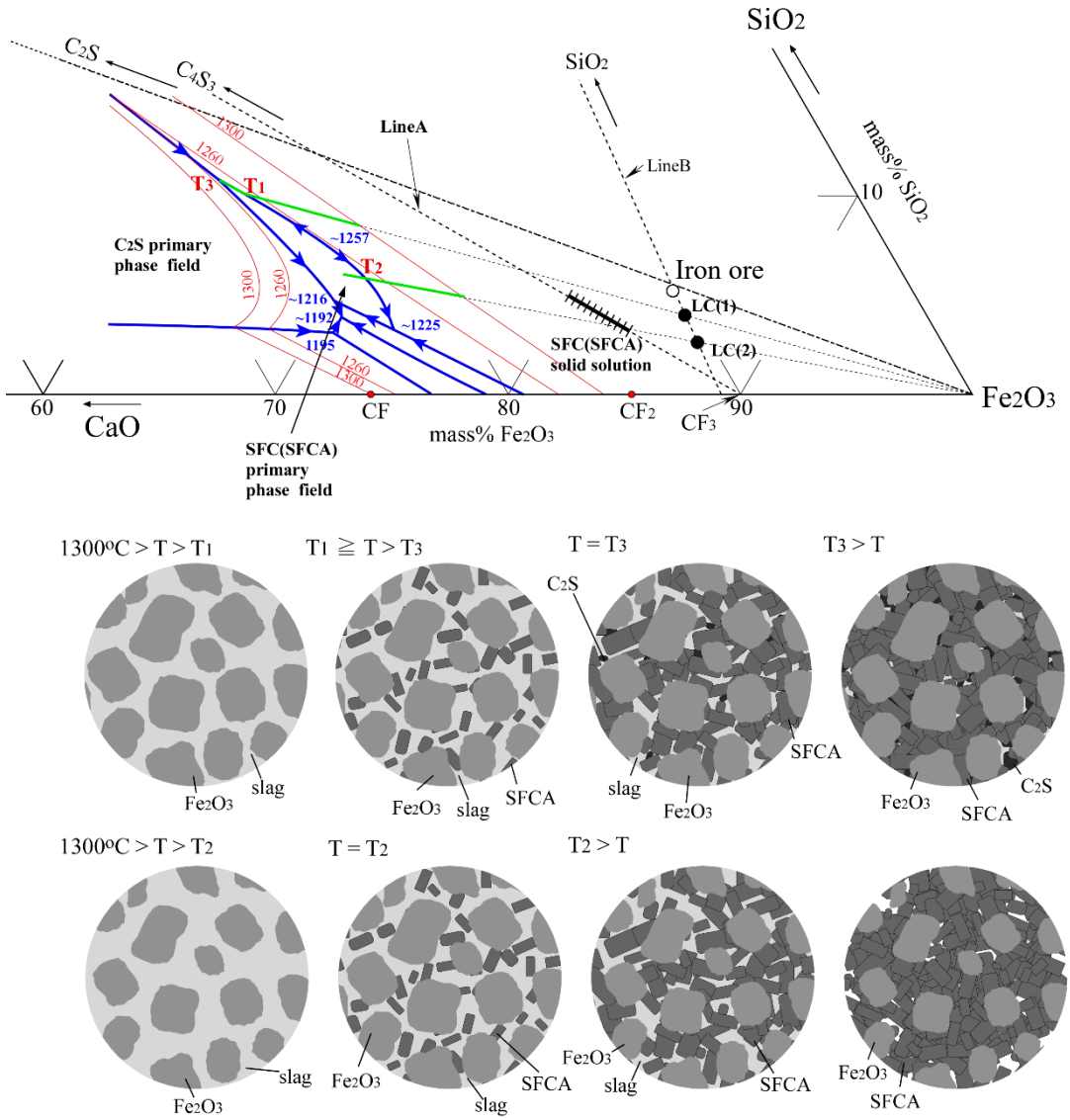

FIG 8 – (a) Phase equilibrium of the iron-rich corner of the CaO-SiO_2-Fe_2O_3 system in air including liquidus, SFC primary phase field, SFC solid solution and the sample composition (Chen et al., 2019). The straight lines connecting $4CaO \cdot 3SiO_2$(C_4S_3) and $CaO \cdot 3Fe_2O_3$ (CF_3), and SiO_2 and sample composition are denoted by Line A and Line B, respectively. (b) Schematic illustration of the equilibrium microstructures for samples having the chemical compositions of LC (1) and LC (2), which are both on Line B. (Hayashi et al., 2022)

CONCLUSIONS

This study investigated the effect of alumina on microstructures of iron ore sinters from the perspective of the phase equilibria of the CaO-SiO_2-Fe_2O_3-5mass%Al_2O_3 system at 1240°C in air including the compositional range of a four-component calcium ferrite (SFCA, SFCA-I), the liquidus isotherm, and the phase equilibria of SFCA and SFCA-I.

The compositional region of SFCA lies on the CF_3-CA_3-C_4S_3 plane and is C/S = 2.77–7.60 for 5 mass%Al2O3. Compared to the SFC composition region with a 0 mass% Al_2O_3 (C/S=2.92–4.32)24), that of SFCA extended in the CF_3-C_4S_3 direction, indicating that the addition of Al_2O_3 contributes to SFCA stability.

The liquid-phase region was divided into a ferrite melt with a high Fe_2O_3 concentration and a silicate melt with a high SiO_2 concentration, both of which shifted to the lower Fe_2O_3 side compared to the liquidus isotherm in the CaO-SiO_2-Fe_2O_3 system (Chen et al., 2019, Dayal and Glasser, 1967).

Unlike the CaO-SiO_2-Fe_2O_3 (0 mass% Al_2O_3) system (Mumme 2003), SFCA-I (SFC-I) was observed in the CaO-SiO_2-Fe_2O_3-5mass%Al_2O_3 system. This suggests that the addition of Al_2O_3 contributes to the stability of SFCA-I. The compositional region of SFCA-I was not on the CF_2-CA_2-C_3S_2 plane owing to the presence of Fe^{2+}.

The aforementioned results imply that an increment in Al_2O_3 concentration in iron ore leads to a decrement in the volume fraction of the bonding phase and that the fraction of the SFCA phase increases, and those of $2CaO{\cdot}SiO_2$ and slag phases decrease in the bonging phase. The SFCA-I phase is also precipitated from the slag with an Al_2O_3 concentration around 5 mass%.

REFERENCES

Chen, J, Shevchenko, M, Hayes, P. C. and Jak, E, 2019, A phase equilibrium of the iron-rich corner of the CaO–FeO–Fe_2O_3–SiO_2 system in air and the determination of the SFC primary phase field, ISIJ Int., 59, pp 795-804.

Chen, J, Cheng, S, Shevchenko, M, Hayes, P. C. and Jak, E, 2021, Investigation of the thermodynamic stability of $C(A, F)_3$ solid solution in the FeO-Fe_2O_3-CaO-Al_2O_3 system and SFCA phase in the FeO-Fe_2O_3-CaO-SiO_2-Al_2O_3 system, Metall. Mater. Trans. B, 52B, pp 517-527.

Cheng, S, Shevchenko, M, Hayes P. C. and Jak, E, 2021, Experimental phase equilibria studies in the FeO-Fe2O3-CaO-Al2O3 system in air, Metall. Mater. Trans. B, 52B, pp 2416-2429.

Dayal, R. R, and Glasser, F. P, 1967, Phase relations in the system CaO-Al_2O_3-Fe_2O_3, Sci. Ceram., 3(1967), pp 191-214.

Hayashi, M, Zhou, D, Iwami, Y, Higuchi, T, Watanabe, T, Endo, R. and Susa, M, 2022, Effect of $2CaO{\cdot}SiO_2$ addition on reaction behavior of iron ore sinters, ISIJ Int., 62, pp 1785-1791.

Hayes, P. C, Chen, J, and Jak, E, 2016, Phase Equilibria Study of the CaO-"Fe_2O_3"-SiO_2 System in Air to Support Iron Sintering Process Optimisation, in Proceedings 10th Int. Conf. on Molten Slags, Fluxes and Salts 2016, Springer, 707-714.

Machida, S, Nushiro, K, Ichikawa, K, Noda, H. and Sakai, H, 2005, Experimental evaluation of chemical composition and viscosity of melts during iron ore sintering, ISIJ Int., 45, pp 513-521.

Mumme, W. G, 2003, The crystal structure of SFCA-II, $Ca_{5.1}Al_{9.3}Fe^{3+}_{18.7}Fe^{2+}_{0.9}O_{48}$ a new homologue of the aenigmatite structure-type, and structure refinement of SFCA-type, $Ca_2Al_5Fe_7O_{20}$. Implications for the nature of the "ternary-phase solid-solution" previously reported in, N. Jahrb. Mineral. Abh., 178, pp 307-335.

Oyama, N, Nushiro, K, Konishi, Y, Igawa, K and Sorimachi, K, 1996, Influence of matrix strength and pore structure on sinter cake strength, Tetsu-to-Hagané, 82, pp 719-724.

Patrick, T. R. C, and Lovel, R. R, 2001, Leaching dicalcium silicates from Iron ore sinter to remove phosphorus and other contaminants, ISIJ Int., 41, pp 128-135.

Patrick, T. R. C, and Pownceby, M, I, 2002, Stability of silico-ferrite of calcium and aluminum (SFCA) in air-solid solution limits between 1240 °C and 1390 °C and phase relationships within the Fe_2O_3-CaO-Al_2O_3-SiO_2 (FCAS) system, Metall. Mater. Trans. B, 33B, pp 79-89.

Sasaki, M and Hida, Y, 1982, Consideration on the properties of sinter from the point of sintering reaction, Tetsu-to-Hagané, 68, pp 563-571.

Scarlett, N. V. Y, Pownceby, M. I, Madsen, I. C. and Christensen, A. N, 2004, Reaction sequences in the formation of silico-ferrites of calcium and aluminum in iron ore sinter, Metall. Mater. Trans. B, 35B, pp 929-936.

Shigaki, I, Sawada, M and Gennai, N, 1986, Increase in low-temperature reduction of iron ore sinter due to hematite-alumina solid solution and columnar calcium ferrite, Trans. Iron Steel Inst. Jpn., 26, pp 503-511.

Takahashi, A, Uchisawa, Y, Sato, H, Watanabe, T, Endo, R, Susa, M, Hayashi, M, 2023, Effect of alumina on the phase equilibria of the Iron-rich corner of the $CaO–SiO_2–Fe_2O_3$ system at 1240°C in air, ISIJ Int., 63, pp 1825-1833.

Tonžetć, I, and Dippenaar, A, 2011, An alternative to traditional iron-ore sinter phase classification, Miner. Eng., 24, pp 1258-1263.

Yang, C. K, Shoji, T, and Takenouchi, S, 1978, Phase relations in the system $CaO-Al_2O_3-Fe_2O_3-SiO_2$ -Mineralogical study on sintered iron ores (2nd report), *J. Min. Metall. Inst. Jpn.*, 94, pp 575-580.